A New True Wireless System for Real-Time Pulse Wave Velocity Assessment

A New True Wireless System for Real-Time Pulse Wave Velocity Assessment

Andrea Valerio, *Member, IEEE*, Irene Buraioli, *Member, IEEE*, Alessandro Sanginario, *Member, IEEE*, Dario Leone, Giulia Mingrone, Alberto Milan, and Danilo Demarchi, *Senior Member, IEEE*

***Abstract*—This work introduces a novel wireless sensor for clinical pulse wave velocity (PWV) assessment. Two pen-shaped acquisition probes have been designed to incorporate a custom printed circuit board (PCB), a rechargeable battery, and a commercial piezoresistive load cell as the sensing element. Using the Bluetooth low-energy (BLE) 5.2 communication protocol, each probe transmits collected data to the USB dongle integrated into the receiving station realized for this application. A graphical user interface (GUI) has been designed to provide clinicians with real-time PWV values and feedback regarding the quality of the acquired signal. To assess the correct behavior of all system units, extensive validation of the developed firmware routines for data transfer and handling was conducted. The reliability of the PWV estimation was assessed in a preclinical study against the gold-standard device for noninvasive PWV (SphygmoCor), showing a robust linear correlation yielding a value of $R^2 = 0.89$. The Bland–Altman plot computed with respect to the reference system reports a mean difference equal to -0.65 ± 0.41 m/s. Finally, electromagnetic compatibility and clinical usability tests were conducted to determine the device's precompliance, according to the clinical safety rules and guidelines described in the IEC-60601 standard for medical devices.**

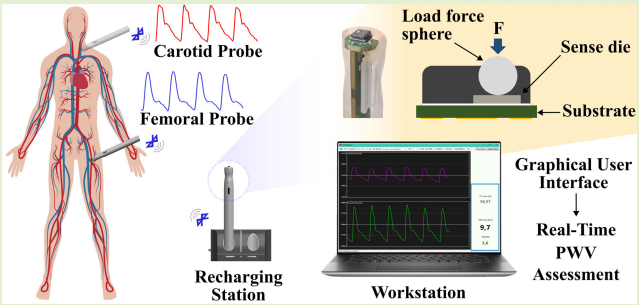

***Index Terms*—Arterial stiffness, Athos device, pulse wave velocity (PWV), vascular aging, wireless physiological monitoring.**

I. Introduction

CARDIOVASCULAR diseases (CVDs) are globally considered the leading cause of death [1], [2], [3]. Arterial stiffness is a multifaceted phenomenon that results from alterations in both the structure and the function of the blood vessel wall [4], [5]. A reduction of the elasticity of vessels leads to elevated systolic blood pressure (SBP) and reduced diastolic blood pressure (DBP). This condition causes a significant workload on the left ventricle, alters coronary perfusion, and promotes chronic arterial inflammation [6]. Arterial stiffness can be non-invasively assessed by evaluating pulse wave velocity (PWV) [7], [8]. As cited by the European hypertension guidelines [9], PWV keeps its predictive and prognostic value even where others prove unreliable and, therefore, is considered the gold standard among stiffness indices and a significant predictor of cardiovascular risk [10], [11]. PWV is the speed at which the pressure wave travels through the cardiovascular system due to the ejection of blood at the end of the systolic phase within the cardiac cycle. The propagation of the arterial pulse can be evaluated between any pair of locations within the cardiovascular system. To date, several devices for the assessment of clinical PWV differ in both the procedure and methodology employed [12]. Concerning the latter, the most widely used and reliable approach is applanation tonometry [10], followed by oscillometry [13], and optical sensors [14]. Depending on the ECG signal's presence, the blood's transit time can also be computed with respect to the R-peak. However, this practice is generally discouraged because it includes the pre-ejection period (PEP) in the

Manuscript received 17 April 2024; revised 28 May 2024; accepted 30 May 2024. Date of publication 24 June 2024; date of current version 1 August 2024. The associate editor coordinating the review of this article and approving it for publication was Dr. Varun Bajaj. *(Corresponding author: Andrea Valerio.)*

This work involved human subjects or animals in its research. Approval of all ethical and experimental procedures and protocols was granted by the University of Turin Bioethical Committee.

Andrea Valerio, Irene Buraioli, Alessandro Sanginario, and Danilo Demarchi are with the Department of Electronics and Telecommunications, Politecnico di Turino, 10129 Turin, Italy (e-mail: andrea.valerio@polito.it; irene.buraioli@polito.it; alessandro.sanginario@polito.it; danilo.demarchi@polito.it).

Dario Leone, Giulia Mingrone, and Alberto Milan are with the Department of Medical Sciences, Internal Medicine and Hypertension Division, University of Torino—AOU Città della Salute e della Scienza di Torino, 10126 Turin, Italy (e-mail: dario.leone@ircc.it; giulia.mingrone@unito.it; alberto.milan@unito.it).

Digital Object Identifier 10.1109/JSEN.2024.3415714

estimation [15]. Commercial PWV devices, which incorporate an ECG acquisition system into their configuration, prevent the incorporation of PEP by conducting a double differential measurement involving the two selected acquisition sites and utilizing the R-peak as a reference point in the procedure. Typical locations for evaluating pulse waves include the femoral, tibial, radial, and carotid arteries, where arterial pulsations are easily detectable [16], [17]. In 2023, the European Society of Hypertension guidelines [18] recommended brachial-ankle PWV (ba-PWV) [19], [20], [21] as a screening tool for hypertension-mediated organ damage [22]. However, carotid-femoral PWV (cf-PWV) is still considered the gold-standard reference in the arterial stiffness assessment [23], [24], [25]. Although cfPWV is a robust measure of vascular aging [26], [27], it is not available in many research studies for a variety of reasons, including financial constraints [3], [7], lack of access to the specialized equipment needed to measure it, and the absence of trained personnel. In 2021, the Athos (Arterial stiffness faithful tool assessment) device was created to overcome the barrier of high equipment costs and usability that have restricted the adoption of this technique within clinical settings [28], [29]. Thanks to its two prototypal high-resolution MEMS force sensors and a dedicated graphical user interface (GUI), this system provides real-time feedback to the user and fully reliable offline cf-PWV assessment. Following the Artery Society guidelines, a clinical validation study involving 90 healthy volunteer subjects was carried out to assess the accuracy of the device [30] in comparison to the established gold standard device for noninvasive cfPWV assessment, SphygmoCor (AtCorMedical in Sydney, Australia) [31], [32]. The Athos device demonstrated a high degree of concordance with SphygmoCor, even under conditions of elevated PWV values, and exhibited satisfactory reproducibility. However, the restricted accessibility of the sensor used in creating the prototype limited its use in clinical practice. To overcome this limitation, the entire system was redesigned using commercial components [33]. That said, the proposed device stands as an entirely novel instrument. Its development results as the culmination of multidisciplinary cooperation with a team of physicians actively engaged in clinical validation. Compared to the first generation, the hardware and software novelties introduced within the proposed device aim to completely transform its portability, streamline usability, and ensure the accuracy of PWV estimation. The primary innovation in terms of hardware is removing the wired connection between the MEMS sensors and the central apparatus that formerly handled data management and transmission to the workstation. Furthermore, to transform the system into an independent device, the ECG connection was also eliminated, significantly enhancing the device's portability. Therefore, a new custom printed circuit board (PCB) powered by a small rechargeable battery was designed to collect the force data and wirelessly transfer them to the workstation hosting the GUI responsible for displaying and processing the pulse waveforms. A new piezoresistive load cell has been selected as the sensing element to capture the arterial pulse. The two pen-shaped acquisition enclosures were revised entirely to hold the mentioned components, ensuring clinicians' easy handling during the PWV assessment. With the decision to incorporate rechargeable batteries into the design, a recharging station was also integrated into the system. The base station, connected to a laptop via USB, acts both as a collector for data streaming and a charging station for the two probes. A USB dongle has been included in the design to handle Bluetooth low-energy (BLE) communication with the acquisition probes and transmit the gathered data to the workstation. The firmware underwent a comprehensive revision. The Bluetooth stack was updated from 4.2 to 5.2 [34], and different routines to manage the data connection, transfer, and reception were implemented to handle the asynchronous transmission from the two probes to the receiving station. The previously designed GUI has been updated, integrating the real-time data display alongside the PWV assessment. The MATLAB algorithm detailed in [29], initially designed for offline extraction of the intersecting tangent points (ITPs) on carotid and femoral waves, was modified to operate in the background, delivering real-time feedback to the clinician.

II. Proposed System

This section guides the reader to a detailed description of the proposed system's design, application, and validation phases. Section II-A details the hardware conceptualization and realization of the custom PCB of the two probes and the recharging station constituting the device. Moreover, the description of the 3-D-printed enclosures of the probes and recharging station is also provided. Then, Section II-B2 reports the firmware routines implemented for managing the connection, the data transfer, and the data management between the acquisition probes, the BLE charging station, and the workstation responsible for providing a real-time PWV assessment to the clinical operator. Section II-C details the GUI and the software algorithm used to manage the commands provided by the user and the real-time estimation of PWV. Section II-D describes the tests performed to assess the power consumption of the probes and the synchronization procedure. Finally, Sections II-D4 and II-E present the procedure used to perform the PWV assessment and the tests conducted to verify the device's compliance according to the clinical safety rules and guidelines described in the IEC-60601 standard for medical devices.

A. Hardware

1) Acquisition Probes: The proposed device consists of three primary units: two probes utilized for data collection and a charging station. The probes, one for the carotid site and one for the femoral site, are intended to be two autonomous devices communicating with the central station through the BLE communication protocol. Since the two probes are identical from a hardware standpoint, the following explanation will pertain to both. As depicted in Fig. 1, each probe consists of three major components: a pen-shaped enclosure containing the sensor used to capture data [see Fig. 1(a)], a custom PCB created for this application [see Fig. 1(b)] and the rechargeable battery used to power the board [see Fig. 1(c)]. The PCB includes the STM32WB15CC (STMicroelectronics, Shanghai, China), a 32-bit multiprotocol wireless and ultralow-power device that embeds an RF subsystem that communicates with

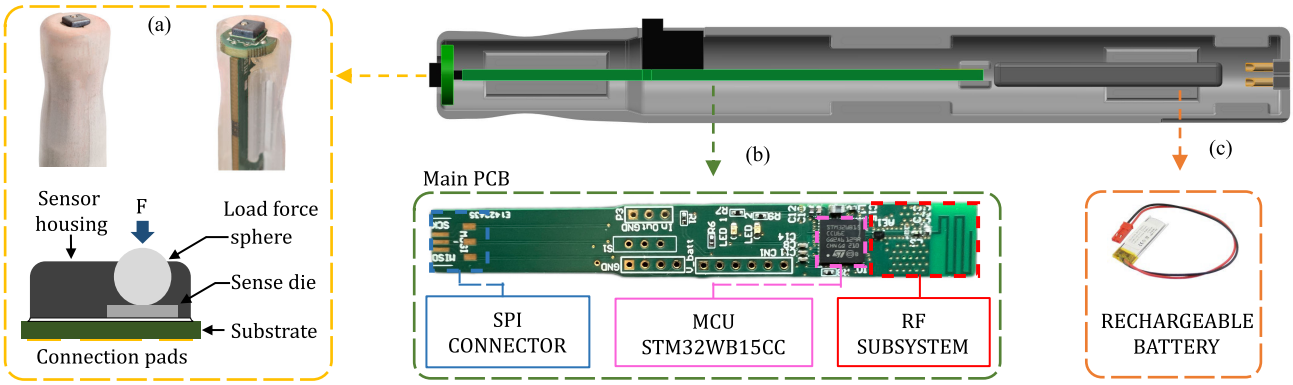

Fig. 1. Acquisition probe overview. (a) Encapsulated load cell used for pulse wave detection. (b) Custom PCB designed to collect and transfer data. (c) Rechargeable polymer lithium-ion battery.

a microcontroller unit (MCU) including an Arm Cortex-M4 CPU (CPU1) where the host application runs [35]. The RF subsystem comprises an RF analog front end and a specialized Arm Cortex-M0+ microcontroller (CPU2) compliant with the BLE SIG specification 5.2. It implements the entire BLE stack, restricting the CPU1's interface to high-level exchanges. Two LEDs, red and green, respectively, have been included in the board's design to provide the user with feedback on the proper reading of the sensor and the BLE connection status. A single ON/OFF switch has been placed on the board to power ON (or OFF) the device. The STLQ020 [36] (STMicroelectronics, Shanghai, China) linear voltage regulator has been included to produce 3.3 V from the initial 3.7 V given by the chosen battery when the board is turned on. The power source used for this device is the LP401235 (Cellevia Batteries), a rechargeable polymer lithium-ion battery [37]. This model was selected for this application because the battery's recharging ability allowed us to minimize its nominal capacity 120 mAh and, as a result, its size and weight, providing the correct voltage to power the board and the sensor. Two external oscillators were employed according to the specifications reported in [35] and [38] concerning hardware development for RF applications. The NX2012SA low-speed external (LSE) oscillator [39], with 32.768-kHz frequency, was used for the RTC subsystem. The 32-MHz crystal oscillator NX2016SA-32M-EXS00A-CS06465 was chosen as the high-speed external (HSE) clock source [40]. This latter is required by the MCU to trim the RF subsystem responsible for managing BLE activities. The mentioned crystal was selected based on the criteria outlined in the microcontroller datasheet [35]. Moreover, it is characterized by a frequency tolerance of 10 ppm (at 25°), which ensures a low drift during data acquisition sessions. The FMAMSDXX005WCSC3 (Honeywell, United States) load-cell has been selected for pulse wave detection [41]. The small form factor (5 × 5 for the base, 2.15 mm for the height), low-power consumption (about 14 mW), the reduced force range, and low costs made it an ideal solution for our application. As depicted in Fig. 1(a), this micro force sensor is actuated by direct mechanical coupling through a stainless steel sphere mounted directly over a silicone sense die. This off-the-shelf, piezoresistive-based force sensor provides a digital output (12-bit data output) for reading force values over the specified full-scale span. A 5-N sensitivity range was chosen from those commercially available to have the sensor dynamics closest to the force values exerted by the arterial pulse passage. Achieving consistent and precise results hinges on the correct sphere alignment and accurate sensor mounting. The sphere transfers the load through a specific point of contact. When this contact point is inconsistent or not perpendicular, it can cause the sphere to exert pressure or friction against the sensor housing, leading to a potential shift in the sensor's output. For this purpose, the load cell has been soldered onto a 1-cm diameter circular PCB. This setup guarantees the sensing sphere's proper alignment along the pen-shaped enclosure's longitudinal axis when the sensor is inserted. Moreover, it serves the dual purpose of powering the sensor and establishing a connection with the main PCB through the serial peripheral interface (SPI) communication protocol. Multiple factors were taken into account during the design of the probe enclosure. Specifically, its shape and dimensions depended on the size of the battery and the custom PCB. For this reason, the PCB and battery dimensions have been reduced as much as possible. The enclosure section close to the sensor was shaped differently to simplify the operator's handling. In particular, the carotid probe was intended to be handled like a pen, whereas the femoral probe was designed to be held between two fingers. Thus, stable simultaneous deployment of sensors becomes feasible, resulting in enhanced and more steady signal acquisition. A series of indentations on the enclosure's side aids the operator in correctly positioning the unit within the charging base. The interface connections are situated on the lower portion of each probe. Specifically, two of the four available pins connect the probe's battery and the circuit within the charging station. The two remaining pins enable a physical linkage between the two probes as a sensing solution to distinguish if they are connected. This solution will be explained later in the acquisition startup routine.

2) Charging Station: The charging base realized for this application represents the central fulcrum of the device. It can be divided into three main sections: the enclosure, the MB1293 USB dongle (STMicroelectronics, Shanghai, China) used to manage the BLE communication and the dedicated PCB built to perform the battery charging inside the probes and the circuit used to perform the acquisition startup. The structure of

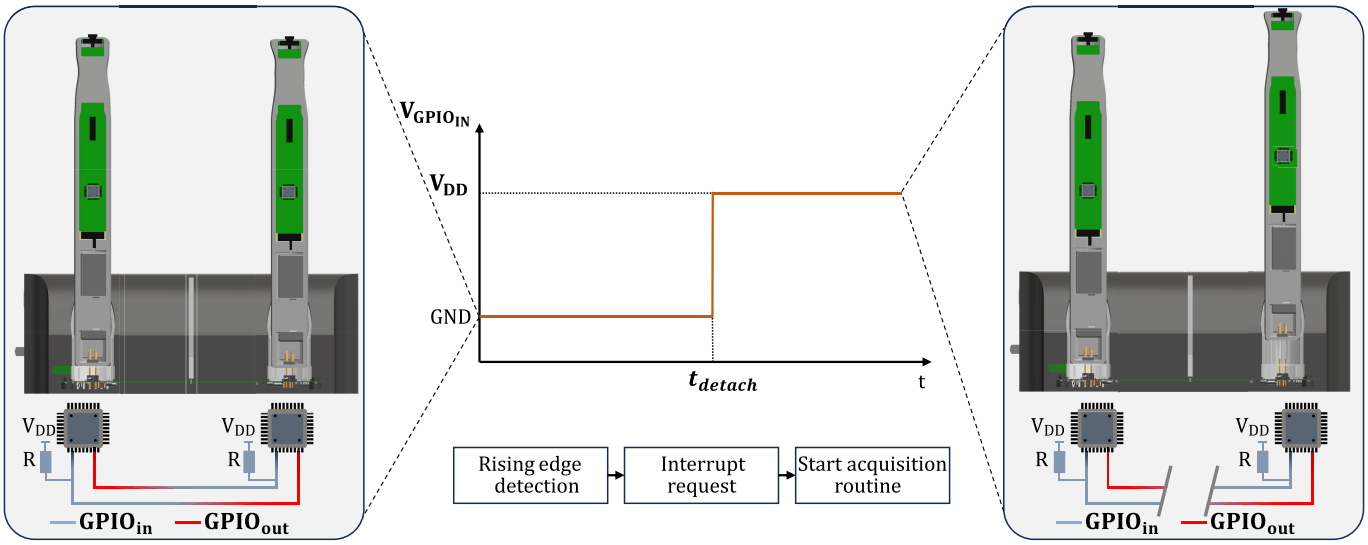

Fig. 2. Recharging station designed for the tested device. The hardware solution relies on bidirectional sensing between the two MCUs embedded in the acquisition probes, enabling a synchronous initiation of the acquisition process. When one of the components is disconnected from the base, it prompts the initiation of the acquisition process. The USB-Dongle, integrated into the main PCB within the base station, enables BLE communications among all system components.

the charging base presents two slots, one for each probe, and a set of LEDs that give the user an indication of the battery recharge. The inner surface of the housings has been shaped to complement the geometry created on each probe to ensure their proper position within the charging base. The connection between the PCB and the bottom part of each probe has been realized using a four-pin spring-loaded header. This solution allowed us to build a more reliable contact with the charging and synchronization circuit. The charging circuit consists of the MCP73831 integrated circuit (Microchip, Shanghai, China) [42]. Through a specific resistor linked to the mentioned integrated circuit, the charging current has been set according to the datasheet requirements of the connected battery. According to [37], a 68-kω resistor has been selected for this purpose, setting a recharge current of 16 mA. The circuit employed for the synchronous start of acquisition is based on the bidirectional sensing of the two probes. When connected, each probe can detect whether the other gets detached from the base. Connecting two pins between each slot made it possible to couple the microcontroller on each probe with the other. Two general-purpose inputs/outputs (GPIOs) have been involved in this process: One was configured in input mode and the other in output mode, depicted, respectively, in blue and red in Fig. 2. Both GPIOs in output mode have been set to provide a low logical state. The GPIOs set as input have been programmed to trigger an interrupt when the transition from the low to the high logical state occurs (see Fig. 2). The interrupt is enabled when the user presses the play button on the graphical interface. A pull-up resistor, placed on each line connecting the two MCUs, makes the transition from the low to the high logical state possible when one of the two probes gets disconnected from the base. As introduced earlier in this section, the BLE communication and data transmission are managed by the USB dongle manufactured by STMicroelectronics (Shanghai, China). The dongle hosts an STM32WB55CG MCU [43], a low-power 32-bit device with a dual-core Arm Cortex-M4/M0+ architecture with similar characteristics to those previously described microcontroller used for the probes. The dongle has been coupled to the PCB via a USB connector mounted on this latter. The ensemble has been further connected by cable to one of the 5-V-powered USB ports on the workstation running the graphic interface for real-time PWV assessment. Section II-B will describe the communication protocol used to handle data transmission.

B. Firmware

The first step in developing the BLE protocol is the implementation of the routine responsible for connecting all the components constituting the proposed device. The reference roles within the BLE protocol are *central* and *peripheral*. In our project, the dongle is the central device; it acts as the master during the connection process and establishes the physical layer connection. On the other hand, the two probes perform as peripheral units; they serve as slaves during the connection process and are responsible for accepting the physical layer connection.

1) Connection Routine: Based on the information presented in Section II-A2, a connection routine was built to identify and connect the two peripheral units with the core unit. This operation begins with the central unit (dongle) scanning the two peripheral units engaged in the advertising phase and enabling the connection. The scan phase (with a *white-list* to filter undesired devices) continues until the connection units are located. Once discovered, the connection procedure proceeds progressively, first establishing contact with the carotid probe and then with the femoral probe. The main criticality identified during the development of this algorithm is the identification of the connection parameters. The selection of the latter, in accordance with the timing constraints provided by STMicroelectronics [44], [45], enabled the establishment

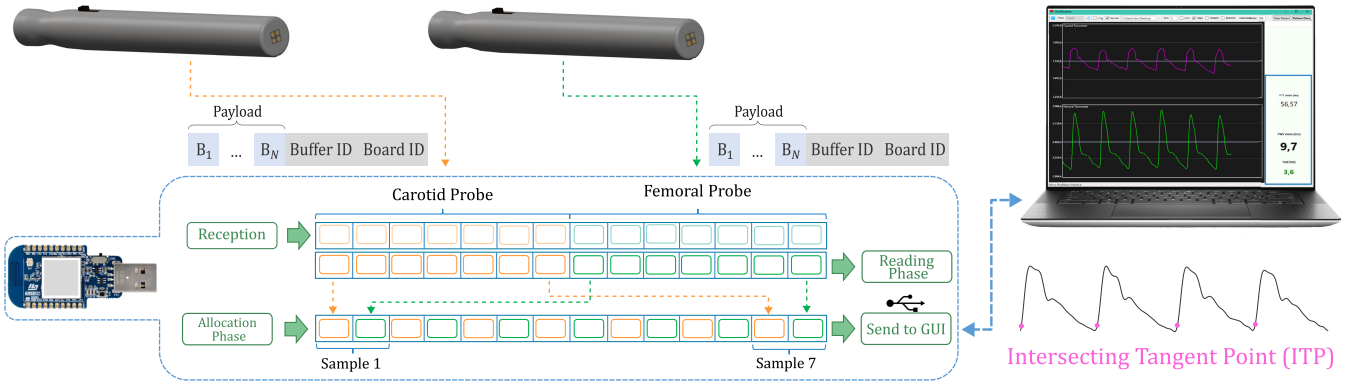

Fig. 3. Schematization of force data management. BLE payloads sent by the acquisition probes are received and allocated into a circular buffer by the USB-Dongle. The samples are reorganized and sent to GUI via a USB connection for real-time processing.

of the two connections and ensured the correct transfer of the acquired data in real-time [32], [46].

2) Data Transfer: The data transfer protocol represents a fundamental part of developing a device for the real-time acquisition system. The user initiates data transfer using commands accessible via the GUI. The command to *start* (or *stop*) data acquisition is forwarded by the central unit (dongle) to the two peripheral units. After receiving the command, each board begins reading the sensor. A four-wire bidirectional SPI communication protocol connects the load cell to the mentioned MCU. The sensor is programmed to work with a sampling frequency of 200 Hz, enabling the acquisition of 12-bit force data output each 5 ms. A circular buffer structure was chosen to allocate the data and subsequently send them into a BLE packet structured as follows.

1) *Bytes 1–14:* Contain the samples acquired by the sensor.
2) *Byte 15:* It is a progressive value representing the current BLE packet filled with force data.
3) *Byte 16:* It can be either 1 or 2 according to which probe is transmitting the data.

3) Data Management: The next step in the development process of the device is the implementation, on the central unit, of a procedure for managing and processing received data before its transmission to the laptop. When dealing with the reception problem, it is important to note that, besides the transmission phase of the acquisition's *start* command, there is a misalignment between the central unit and peripheral devices. This misalignment happens because the central unit cannot receive data from the peripherals simultaneously. The routine is divided into three major phases.

1) *Read Phase:* It involves the reception of the BLE data packets sent by each peripheral. Based on the last two bytes, the packet sequence number is sorted, and data are assigned to the proper sensor (carotid or femoral buffer).
2) *Allocation Phase:* It involves the copying of data within a circular buffer divided into 28 bytes as follows.
   a) *Bytes 1–14:* Contain the data from the carotid probe.
   b) *Bytes 15–28:* Contain data from the femoral probe.

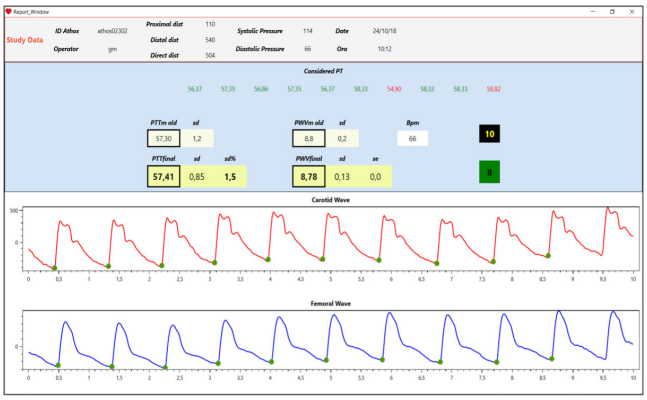

Fig. 4. Report generated at the end PWV study.

Once the buffer is full, the samples within are alternately reordered according to the diagram in Fig. 3.
3) *Transmitting Phase:* The data set is sent to the workstation for real-time display via a USB connection.

C. Graphic User Interface for PWV Assessment

Once the system's physical structure and communication protocols were defined, we implemented the graphic user interface for controlling the device from a computer using Visual StudioCode. The software is designed to execute three distinct functions. The first task involves recognizing the USB-Dongle responsible for establishing the connection and managing data communication with the acquisition probes. Second, the software interprets and transmits user commands to the peripheral units. Finally, the BLE packets containing gathered data are reorganized for real-time plotting and are processed for PWV calculation. The patented algorithm [47], originally developed and detailed in [29], has been adjusted to operate in the background, providing updated values of pulse transit time (PTT), PWV, and corresponding standard deviation every 1.5 s. Fig. 4 shows the comprehensive report generated when the acquisition is terminated. This report represents a summary of the PWV test just run and considers the last 10 s of the waves, as foreseen in the standard procedure. The report includes the subject's personal information, the PTT and PWV values, and, finally, the acquired carotid and femoral pulses with the related ITPs.

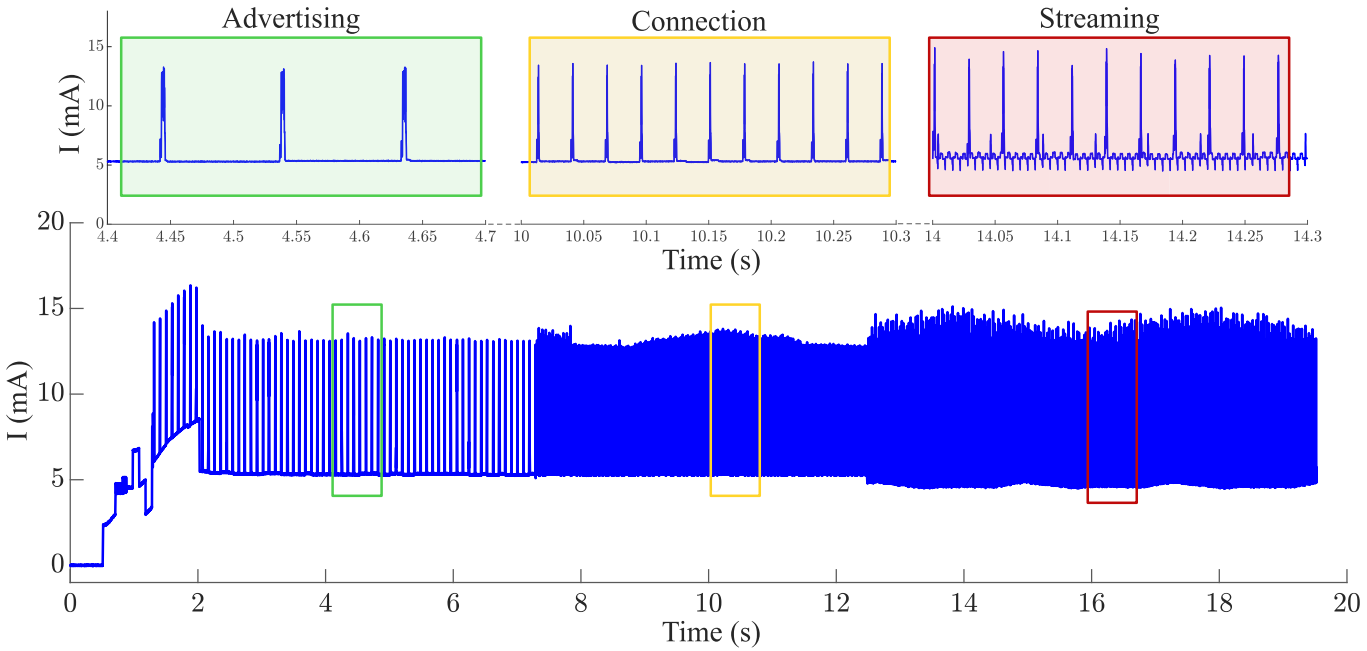

Fig. 5. Current absorption of the acquisition probe during the different function modalities: advertising, connection, and streaming.

D. Testing Phase

Section II-D introduces the setup employed to conduct a comprehensive series of tests to evaluate the device's performance.

1) Setup for Synchronization Assessment: A crucial aspect for ensuring a trustworthy measurement is the achievement of precise synchronization in the reception of the initial data acquisition *start command* from peripheral units. Even a minor deviation of a few milliseconds could introduce uncertainty and reduce the measurement's reliability. Synchronization was assessed using an oscilloscope. One accessible GPIO pin was configured to be toggled to a high logical state as soon as the *start command* is received. By establishing a connection between the oscilloscope probes and the specified and the mentioned GPIO, it became feasible to visually see and quantitatively determine the time delay associated with the reception of the start command by the two probes.

2) Setup for Power Consumption Evaluation: Given the integration of a rechargeable battery within the acquisition probes, we analyzed the absorbed current during each device's operation phase. For this purpose, we used the DMM7510 digital graphical multimeter. We set a sampling frequency of 10 kHz to detect the BLE module activity.

To perform the measurement, the multimeter probes were placed on power lines connecting the battery to the PCB. An ensemble of three acquisitions lasting between 3 and 5 min was collected, and data were further analyzed offline using MATLAB. The duration of each acquisition was chosen to replicate the average time used to conduct the PWV study in a clinical setting. Fig. 5 displays a snapshot of the four main working modalities of the probe.

1) *Initialization of the Probe:* When the probe is switched on, the microcontroller is initialized along with the load cell. If this latter is successfully read, the LEDs are switched on and off to give feedback to the user.
2) *Advertising:* After the initialization, the probe starts the *advertising phase* to inform the charging station about its presence.
3) *Connection Establishment:* Once the dongle initializes the BLE link with the two probes, all the units enter into a stable connection status. Both the central and peripheral units regularly assess the status of the other to confirm ongoing activity.
4) *Data Stream:* Every 35 ms, a new circular buffer is filled on the probe and sends a notification command to the BLE stack that prompts the transmission of the packet during the subsequent available connection interval.

The averaged absorbed current values were evaluated for the mentioned working conditions. We employed the highest current value to derive the discharge curve and estimate the actual battery life of each probe. Parallelly, we assessed the minimum voltage so that all components could work properly in the worst case scenario. The discharge curve was obtained through an equivalent circuit consisting of the battery, the voltage regulator on the PCB, and a resistor equal to 560 Ohm. The latter was dimensioned to represent the total consumption of the probe in the streaming mode with an absorbed current of 5.9 mA when supplied with a regulated voltage of 3.3 V. This setup was made according to datasheet specifications, under constant load conditions and with a discharge current at most 24 mA. The battery voltage was monitored using the NI USB-6259 board (National Instruments) [48] for the entire experiment. Data was acquired via serial interface using MATLAB with a sampling rate of 1 Hz.

3) Setup for BLE Data Transfer Analysis: This section presents the setup used to evaluate the transmission efficiency of BLE packets. Both probes are programmed to transmit a signal with a sawtooth shape to evaluate better the result of the data management protocol developed on the dongle. The data are saved through the previously described dedicated

Fig. 6. Experienced physician performing PWV assessment using the Athos system.

GUI, in *.bin* format, and analyzed offline in the MATLAB environment. A single 20-minute acquisition was performed, and then the order of packet arrival, correct reordering of simulated samples, and any packets lost during transmission were evaluated.

4) PWV Assessment: To assess the efficacy of the presented system, a clinical trial was conducted at the "Città della Salute e della Scienza" Hospital in Turin, Italy. Following the experimental protocol approved by the" University of Turin Bioethical Committee," described by Buraioli et al. [29], ten healthy volunteers were recruited to compare the results gathered using the proposed device with respect to those of the SphygmoCor, available in the hospital. Before commencing each data capture session, informed consent was obtained from every participant. Then, two experienced clinical operators conducted the data collection process to ensure the acquisition of high-quality and stable signals, Fig. 6. Following the standard practice for clinical PWV evaluation detailed in [9], each participant involved in the study underwent three acquisitions using both systems, with the clinical operators alternating the usage of both devices from subject to subject. Finally, a representative PWV value is derived for each individual by calculating the average data acquired from the three acquisitions collected using both systems.

E. Precompliance CE Tests

1) Electromagnetic Compatibility: The set of tests was carried out inside an anechoic chamber in the facility equipped for performing immunity tests up to a frequency of 6 GHz. In accordance with the requirements of IEC 60601-1-2, the device was placed on a rotating table inside the chamber at a distance of 3 m from the antenna used to generate the electromagnetic field used in the test. Given the electric field strength of 3 V/m, immunity was evaluated over three frequency ranges: 80–800 MHz, 800 MHz–2.7 GHz, and 2.7–6 GHz. Each range was tested by varying the orientation of the device with respect to the antenna on each of the four sides for a total of 12 tests. In each test, observations were made to determine if the application of the disturbing field resulted in any changes in the force values recorded at no-load by the load-cell sensor on the probes. Additionally, any loss of data was monitored during transmission between the two probes and the dongle, which was also placed inside the chamber, as shown in Fig. 7.

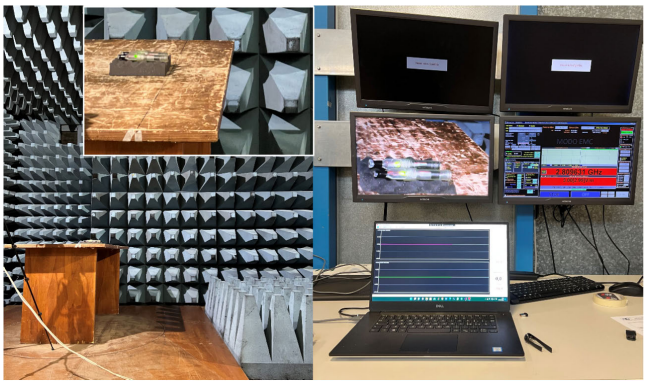

Fig. 7. Anechoic chamber used to assess the electromagnetic compatibility of the system.

2) Clinical Usability: The clinical evaluation of the device was carried out at the A.O.U. Città della Salute e della Scienza di Turin to verify the effectiveness, efficiency, and ease of use of the Athos system. This assessment was overseen by an external certified consultant to ensure accuracy and compliance with the guidelines outlined in IEC 62366-1:2015 and IEC TR 62366-2:2016 concerning the application of usability engineering to medical devices. These standards focus on the importance of understanding user needs, translating them into design specifications, and conducting usability testing to ensure that devices are safe, effective, and user-friendly. Moreover, they emphasize the identification, assessment, and mitigation of use-related hazards to minimize risks to users. In the investigation process, five specialized clinical operators and the project's technical referees were involved in supervising operations and collecting user feedback on the device.

Each operator, aged between 28 and 47 years with varying degrees of experience in PWV measurement, performed an ensemble of three acquisitions with the proposed acquisition system. The physicians who took part in this test filled out an interview report guided by questions posed by the team. To avoid interaction bias, the moderators briefly described the report to the participants, and therefore, it was autonomously compiled using a PC or tablet interface. The users provided feedback on a graded scale ranging from 0 to 4, in which a lower rating corresponds to a favorable opinion of the device.

III. System Assessment

In this section, the results of the introduced tests are reported and discussed, starting with the synchronization of the peripheral units, the current absorbed by each probe, the validation of the data exchange routine, and, finally, the results of the pre-compliance tests carried out on the device.

Synchronization: Using the setup described in Section II-D1, the synchronous start of the acquisition was evaluated. As a first step, an evaluation of the time lag related to the settings of the BLE stack was performed. Given

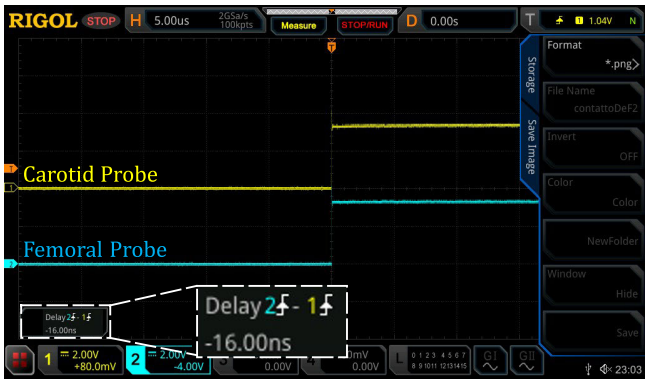

Fig. 8. Observed delay between carotid (yellow) and femoral (blue) probes at the acquisition startup using the proposed hardware solution.

TABLE I
AVERAGED CURRENT ABSORPTION IN DIFFERENT WORKING MODALITIES

	Advertising	Connection	Streaming
Absorbed Current (mA)	5.49	5.48	5.90
Expected Battery Life (h)	21.8	21.8	20.3

a connection interval ranging between 15 and 40 ms, the observed lag was 20.94 ms. This delay can be attributable to the BLE stack transmitting the *start* command within the same connection interval. Therefore, the initial step taken to solve this issue was to find a compromise between parameters. However, this strategy was ineffective, as the average delay value obtained from five tests was 11.56 ms, considered unsatisfactory for this application. Since a software approach did not solve the issue, a hardware solution was chosen. This latter is based on the detachment from the charging station of one of the two peripheral units described in Section II-A2. The synchronization was again evaluated through the oscilloscope, and the result can be seen in Fig. 8. The second approach reduced the acquisition startup delay to a value of 16 ns, considered acceptable for this application. As reported in Section II-A1, a 32-MHz crystal oscillator was selected as an HSE clock source to trim both the MCU and the RF subsystem. The 10-ppm frequency tolerance ensures a low drift during data acquisition sessions. It is important to note that the proposed system is not mentioned for long-term monitoring, and the time required for a single acquisition ranges between 5 and 20 min. Therefore, we assumed the eventual drift to be negligible in the defined operative window. In addition, before starting each session, both probes must be attached to the base station to ensure a synchronous startup; consequently, the clock drift is reset when a new acquisition is started.

Power Consumption: The battery's autonomy introduced in Section II-A1 was evaluated in the laboratory using the setup detailed in Section II-D2. Table I shows the expected autonomy computed by dividing the nominal capacity by the averaged absorbed current values for the defined working conditions.

The minimum value is registered during the connection phase (i.e., 5.48 mA), attributed to the activation of the status LED, RF activity, and ultimately the enabling of sensor

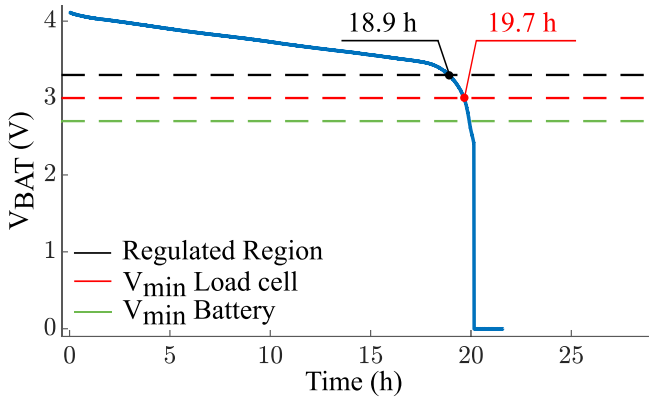

Fig. 9. Discharge curve of the CELLEVIA BATTERY LP401235 under a pure resistive and constant load.

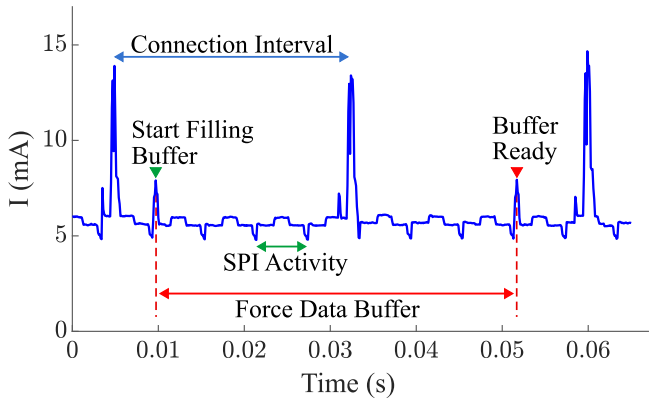

Fig. 10. Events occurring during the streaming mode: BLE connection interval, SPI activity, force data buffer ready to be transferred.

readout. The highest value occurs during the streaming mode (i.e., 5.9 mA), in which the BLE packets containing the force data are sent. Following the trend of the mean value, the standard deviation computed in each working modality assumes the lowest value in the connection phase and the highest when the streaming occurs. Based on these results, we derived the battery's discharge curve (see Fig. 9) to estimate the actual battery life of each probe and the minimum voltage so that all components could work properly. In these conditions, designed to mimic the maximum consumption modality, it took 20.2 h for the battery to get fully discharged, thus matching the expected battery life computed on nominal characteristics (i.e., 20.3 h). However, when evaluating the minimum voltage value to ensure proper operation of the components, we considered the reference voltage values of the integrated components mounted on each probe: the microcontroller [35], the load cell [41], and the linear voltage regulator [36] (equal to 1.7, 3, and 2.75 V, respectively). By selecting the reference value of the low dropout (LDO) to establish a supply voltage within the regulated range of 3.3 V, the autonomy decreases to 18.9 h. However, under these circumstances, each probe has approximately a further hour before reaching the minimum supply voltage required for the load cell to work reliably. Subsequently, we verified the consistency of the BLE activity with respect to the settings chosen for this application. In Fig. 10, a representative window of 70 ms, captured during

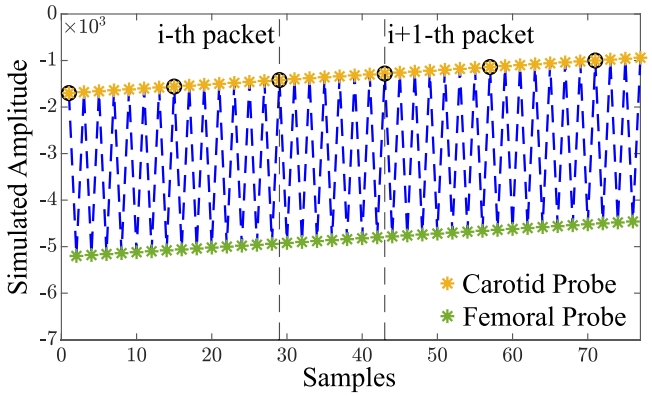

Fig. 11. Result of data management routine in the 20-min acquisition used to validate the data transfer process. No reported cases of lost BLE packets or probe misalignment were observed during this procedure.

the streaming mode, is reported. As it is possible to observe, the variations of the current absorbed by the probe are coherent with the specifications of the BLE protocol and the firmware implemented to read the load-cell sensor. Few regular events alter the baseline as follows.

1) The highest peaks, reaching up to 15 mA, correspond to the transmission of BLE notifications. This operation necessitates the activation of the RF module, albeit for a very brief period. These peaks consistently occur every 28 ms due to the chosen connection interval.
2) The peaks below 10 mA, highlighted in red, indicate when the circular buffer is filled with force data and ready to be sent in the following connection interval. The load cell is programmed to read a new sample every 5 ms. The periodic trapezoidal pattern represents the SPI activity.

BLE Data Transfer Analysis: The last step in evaluating the proposed system is to validate the implemented routines for data management and transfer. In the power consumption section, Fig. 10 allowed us to visualize the consistency of the BLE and SPI activity with respect to the proposed configuration of each acquisition probe. In this section, the emphasis is directed toward the activities of the dongle related to receiving data and its subsequent handling for processing and display in the GUI. To do so, each probe is programmed to transmit a signal with a known growing shape. A representative window showing the results of the data management routine is reported in Fig. 11. The samples are color-coded according to the probe ID identifying the unit responsible for transmitting the data packet: yellow for the carotid and green for the femoral probe.

A black circle has been added to highlight the beginning of each data buffer sent to the GUI. By utilizing signals with a predetermined periodic pattern, it became feasible to confirm the reordering of samples as detailed in Section II-B3 and to detect any potential data loss, which would manifest as anomalies in the plot. The potential risk of data loss was assessed through a 20-min data acquisition session. During this procedure, the quantity and synchronization of BLE packets between probes have been monitored at consistent 20-min intervals. No reported cases of lost BLE packets or probe misalignment were observed during this procedure.

TABLE II
RESULTS OF THE VALIDATION PROCESS

Subject	Athos		Sphygmocor	
	PWV	$\sigma\%$	PWV	$\sigma\%$
1	6.5 ± 0.8	12.3	6.5 ± 0.8	12.3
2	8.0 ± 0.5	6.3	8.8 ± 0.5	5.7
3	6.2 ± 0.2	3.2	6.8 ± 0.2	2.9
4	7.7 ± 0.5	6.5	8.8 ± 0.5	5.7
5	6.1 ± 0.2	3.3	6.8 ± 0.2	2.9
6	5.1 ± 0.1	2.0	5.9 ± 0.1	1.7
7	7.1 ± 0.4	5.6	7.4 ± 0.4	5.4
8	4.1 ± 0.3	7.3	5.3 ± 0.3	5.7
9	5.4 ± 0.8	14.8	5.4 ± 0.3	5.6
10	4.8 ± 0.6	12.5	5.8 ± 0.6	10.3

Notes: PWV, averaged values of the three acquisitions executed during the data collection, $\sigma\%$, percentage of the standard deviation.

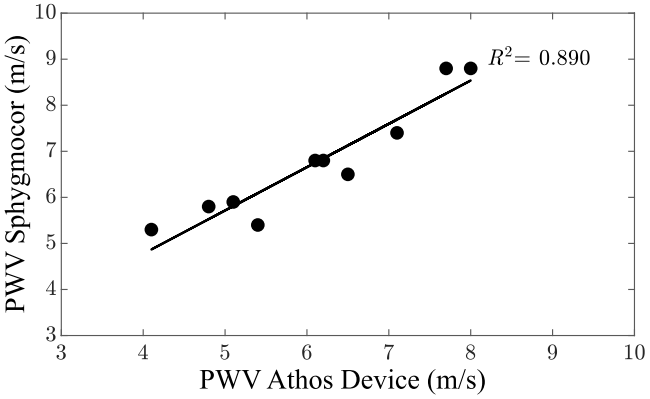

Fig. 12. Scatter plot confronting the averaged PWV values obtained for each recruited subject. A linear regressive model fit on the available data points shows a strong linear correlation between the two devices.

PWV Assessment: Table II reports the averaged PWV values acquired across all examined subjects and the associated standard deviations. The accuracy of the proposed system was assessed by examining the correlation of PWV values between the two instruments and by analyzing the measurement agreement across the study population. The scatter plot is shown in Fig. 12 exhibits the mean PWV values for each participant. A linear regression model was employed to quantify the relationship between measurements, and its quality was assessed using the determination coefficient (R^2). The robust linear correlation between the two devices is evident from the dispersion of the actual data points around the model's best-fit line, as indicated by the coefficient R^2, which yielded a value of 0.89. The Bland–Altman plot reported in Fig. 13 represents the agreement distribution between the two instruments. As shown, the PWV mean difference is about -0.65 ± 0.41 m/s. The comparison between the two devices reveals that the proposed system yields PWV values that closely match those of the gold standard. The reliability of the measurements was validated by the regression model, which highlighted their strong linear correlation, and by the Bland–Altman plot, which indicated a bias well below the 1-m/s limit stipulated by the guidelines for an excellent cfPWV estimation [53].

A. Precompliance CE Test

This section outlines the results of the precompliance CE test conducted on the Athos system.

TABLE III
REFERENCE SYSTEMS FOR NONINVASIVE PWV ASSESSMENT

Device	Disadvantages	Advantages	Execution mode	Sensor	Reference
Arteriograph	High sensitivity to motion Cuff Placement Time-consuming Brachial PWV	Portability Operator indipendence	One-step	Arm pressure cuff	[49], [50]
Complior	Operator dependent Low comfort High sensitivity to motion	Excellent accuracy	One-step	Piezoelectric mechanotransducers	[51], [52]
Sphygmocor	Operator dependent Need of ECG Reduced portability Time-consuming Elevated costs	Excellent accuracy	Two-step	Applanation tonometry	[25], [29], [30]
Pulse Pen	Operator dependent Need of ECG according to the selected setup	Portability Excellent accuracy	One or two steps	Applanation tonometry	[12], [25], [52]
Athos	Operator dependent	Portability Excellent accuracy Ease of use Real-time feedback	One-step	Piezoresistive load cell	Present work

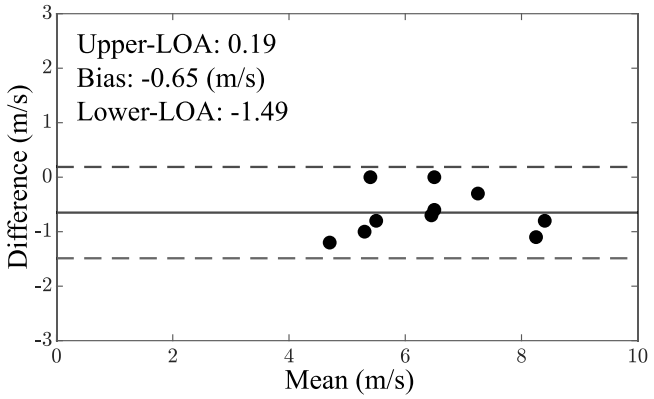

Fig. 13. Bland-Altman plot of the difference between the performances given by the SphygmoCor and the proposed device.

1) Clinical Usability: As stated in Section II-E2, the clinical usability was assessed according to IEC 62366-1:2015 and IEC TR 62366-2:2016 concerning the application of usability engineering to medical devices. The evaluation considered key aspects such as patient preparation, system setup, and application during PWV assessment. In addition, safety measures, cleaning, and storage procedures were examined to mitigate user-related risks and preserve the device's integrity. In general, during the simulated use of the device by participants, no usage or technical errors occurred. All users measured according to the proposed workflow without encountering significant difficulties, even when the operator had no prior experience with the device. The results of their experience were evaluated through a guided response questionnaire using a scale from 0 to 4, where a lower score corresponds to a favorable opinion of the device. The overall scores can be considered very positive, as most of them fall within the nonrisk zone (scores equal to or lower than one), indicating a generally favorable opinion of the device.

2) Electromagnetic Compatibility: The outcome of the tests for RF electromagnetic emission, according to CISPR 11, classifies the Athos acquisition system in Group 1, Class A, defining its RF emissions in a way that does not cause any interference for electronic systems in the vicinity. From an electromagnetic compatibility perspective, the device is deemed suitable for the application of interest.

B. Benchmark Comparison

After examining the performance of the proposed device in Section III, we now contextualize our findings within the existing literature. Given the extensive field of noninvasive PWV assessment, we selected the clinical devices considered the most pertinent for our comparative analysis. Specifically, we have selected the Arteriograph, Complior, Sphygmocor, and Pulse Pen, as they are clinically graded, commercially available, and utilize diverse sensing mechanisms. In Table III, we report the main advantages and disadvantages of the commercially available systems routinely used in the diagnostic clinic environment according to the available literature. Our evaluation encompasses factors such as sensitivity to motion, level of operator independence, portability, preparation time required for patients, and comfort levels. Utilizing a single oscillometric brachial cuff, the Arteriograph (TensioMed, Hungary) stands out for its portability and operator independence, making it versatile for various settings [13], [20]. However, its sensitivity to motion and cuff placement may affect accuracy [49], [50]. In contrast, the Complior (ALAM Medical, France) system records arterial wave pulses concurrently using up to four piezoelectric transducers placed directly on the skin (carotid, femoral, and radial distal arteries) [53]. Despite being acknowledged as a gold-standard device for noninvasive PWV assessment, it is operator-dependent and may lack comfort during use [51], [52]. Similar to the Complior, the Sphygmocor offers unparalleled accuracy but requires an ECG, is less portable, and has higher costs. Moreover, it requires a high level of operator expertise in peripheral signal acquisition [25], [29], [53]. PulsePen (DiaTecne, Italy) detects pressure wave-

forms at the carotid and femoral arteries either simultaneously or sequentially using applanation tonometry. It comprises two small portable tonometers and a compact ECG unit [12], [25], [52]. Starting from the device's main drawbacks reported in the literature, we created a low-cost, noninvasive, yet reliable system. Numerous efforts were made to improve portability and ease of use by removing the acquisition system for ECG and introducing two wireless and lightweight sensing probes. Nonetheless, it is essential to address the limitations that emerged in this study. First of all, the small sample size is attributed to the restricted number of participants. It is essential to note that the preclinical trial enabled the evaluation of the hardware and firmware updates implemented in the device, as well as the feasibility of the new sensor used for PWV assessment. Additionally, the disparity between the sensor dynamics, ranging from 0 to 5 N, and the forces involved in the arterial pulse passage might reduce sensor resolution. Nevertheless, upon analyzing the accuracy of PWV estimation, the comparison with the gold standard device did not unveil any significant concerns regarding the measurement's reliability while simultaneously achieving all goals regarding portability and enhanced usability. Thus, considering all the aforementioned factors, our prototype closely aligns with the current state-of-the-art literature. Moreover, it completely fulfills its intended purpose in noninvasive PWV assessment.

IV. Conclusion

In this work, we presented a wireless device to provide a real-time cfPWV assessment. We re-engineered the entire hardware of the device to improve the portability and ease of use with respect to the former system. The prototypal sensor originally employed in the Athos device [54] was removed in favor of a commercial piezoresistive load cell that proved to be well-suited for detecting arterial pulses. The firmware received an update, and a novel communication protocol was devised to facilitate the interconnection of the units, accompanied by procedures to manage and transfer data. The GUI was improved by integrating real-time PWV assessment. The electromagnetic compatibility test was conducted to verify the system's adherence to medical device design guidelines. Clinical usability was validated by five clinical operators with varying experience in assessing PWV, indicating a generally favorable opinion of the device. The evaluation of PWV estimation accuracy against the gold standard device did not reveal any significant concerns regarding the reliability of the measurement. In conclusion, it was demonstrated that the proposed system effectively enhanced the key aspects that inspired the design of the former device. Improved portability and ease of use were achieved through a redesign of the device on all levels to provide a system capable of broadening the accessibility of this measurement in the clinical environment.

Acknowledgment

The authors would like to acknowledge and thank the participants, researchers, and clinicians for their contributions to this work.

References

[1] T. Sondej et al., "Validation of a new device for photoplethysmographic measurement of multi-site arterial pulse wave velocity," *Biocybernetics Biomed. Eng.*, vol. 41, no. 4, pp. 1664–1684, Oct. 2021.

[2] R. A. Xuereb, C. J. Magri, and R. G. Xuereb, "Arterial stiffness and its impact on cardiovascular health," *Current Cardiol. Rep.*, vol. 25, no. 10, pp. 1337–1349, 2023.

[3] D. Li, F. Cao, W. Cheng, Y. Xu, and C. Yang, "Predictive value of estimated pulse wave velocity for cardiovascular and all-cause mortality in individuals with obesity," *Diabetol. Metabolic Syndrome*, vol. 15, no. 1, p. 40, Mar. 2023.

[4] X. Li, H. Du, X. Li, Q. Gao, J. Chen, and X. Chen, "Brachial-ankle pulse wave velocity is associated with intracranial artery calcification in acute stroke patients," *Clin. Neurol. Neurosurgery*, vol. 233, Oct. 2023, Art. no. 107918. [Online]. Available: https://linkinghub.elsevier.com/retrieve/pii/S0303846723003347

[5] G.-Y. Li, Y. Jiang, Y. Zheng, W. Xu, Z. Zhang, and Y. Cao, "Arterial stiffness probed by dynamic ultrasound elastography characterizes waveform of blood pressure," *IEEE Trans. Med. Imag.*, vol. 41, no. 6, pp. 1510–1519, Jun. 2022.

[6] I. Sequí-Domínguez, I. Cavero-Redondo, C. Álvarez-Bueno, D. P. Pozuelo-Carrascosa, S. Nuñez de Arenas-Arroyo, and V. Martínez-Vizcaíno, "Accuracy of pulse wave velocity predicting cardiovascular and all-cause mortality. A systematic review and meta-analysis," *J. Clin. Med.*, vol. 9, no. 7, p. 2080, Jul. 2020.

[7] A. V. Siva Kumar, K. MaheshKumar, K. N. Maruthy, and R. Padmavathi, "Comparision of photo pulse plethysmography module with Mobil-O-graph for measurement of pulse wave velocity," *Clin. Epidemiology Global Health*, vol. 9, pp. 216–220, Jan. 2021.

[8] K. S. Heffernan, D. Charry, J. Xu, H. Tanaka, and J. R. Churilla, "Estimated pulse wave velocity and incident heart failure and its subtypes: Findings from the multi-ethnic study of atherosclerosis," *Amer. Heart J. Plus, Cardiol. Res. Pract.*, vol. 25, Jan. 2023, Art. no. 100238.

[9] I. B. Wilkinson et al., "ARTERY society guidelines for validation of non-invasive haemodynamic measurement devices: Part 1, arterial pulse wave velocity," *Artery Res.*, vol. 4, no. 2, pp. 34–40, 2010.

[10] A. Álvarez-Bustos et al., "Association between pulse wave velocity and frailty, disability, and mortality in community-dwelling older adults," *JACC, Adv.*, vol. 2, no. 5, Jul. 2023, Art. no. 100423. [Online]. Available: https://linkinghub.elsevier.com/retrieve/pii/S2772963X2300282X

[11] M. J. van Hout et al., "Estimated pulse wave velocity (ePWV) as a potential gatekeeper for MRI-assessed PWV: A linear and deep neural network based approach in 2254 participants of The Netherlands epidemiology of obesity study," *Int. J. Cardiovascular Imag.*, vol. 38, no. 1, pp. 183–193, Jan. 2022.

[12] G. Fiori, F. Fuiano, A. Scorza, S. Conforto, and S. A. Sciuto, "Non-invasive methods for PWV measurement in blood vessel stiffness assessment," *IEEE Rev. Biomed. Eng.*, vol. 15, pp. 169–183, 2022.

[13] I. M. Zota et al., "Arterial stiffness assessment using the arteriograph in patients with moderate–severe OSA and metabolic syndrome—A pilot study," *J. Clin. Med.*, vol. 10, no. 18, p. 4238, Sep. 2021.

[14] S. Bichali et al., "Simplified pulse wave velocity measurement in children: Is the pOpmètre valid?" *PLoS ONE*, vol. 15, no. 3, Mar. 2020, Art. no. e0230817.

[15] M. Y. M. Wong, E. Pickwell-MacPherson, Y. T. Zhang, and J. C. Y. Cheng, "The effects of pre-ejection period on post-exercise systolic blood pressure estimation using the pulse arrival time technique," *Eur. J. Appl. Physiol.*, vol. 111, no. 1, pp. 135–144, Jan. 2011.

[16] P. M. Nabeel, S. Karthik, J. Joseph, and M. Sivaprakasam, "Arterial blood pressure estimation from local pulse wave velocity using dual-element photoplethysmograph probe," *IEEE Trans. Instrum. Meas.*, vol. 67, no. 6, pp. 1399–1408, Jun. 2018.

[17] V. P. Rachim, S. Kang, J.-H. Baek, and S.-M. Park, "Unobtrusive, cuffless blood pressure monitoring using a soft polymer sensor array with flexible hybrid electronics," *IEEE Sensors J.*, vol. 21, no. 8, pp. 10132–10142, Apr. 2021.

[18] G. Mancia et al., "2023 ESH guidelines for the management of arterial hypertension the task force for the management of arterial hypertension of the European society of hypertension endorsed by the European renal association (ERA) and the international society of hypertension (ISH)," *J. Hypertension*, vol. 41, pp. 1874–2071, Jun. 2023.

[19] Y. Lu et al., "Global distributions of age- and sex-related arterial stiffness: Systematic review and meta-analysis of 167 studies with 509,743 participants," *eBioMedicine*, vol. 92, pp. 104619–104634, Jun. 2023.

[20] Y. Arita, T. Fukui, N. Ogasawara, and S. Hasegawa, "Clinical implication of the brachial-ankle pulse wave velocity for endovascular treatment," *Indian Heart J.*, vol. 73, no. 5, pp. 650–652, Sep. 2021.

[21] S. Kwak et al., "Associations of brachial-ankle pulse wave velocity with left ventricular geometry and diastolic function in untreated hypertensive patients," *Frontiers Cardiovascular Med.*, vol. 8, May 2021, Art. no. 647491.

[22] K. Stone et al., "Reimagining the value of brachial-ankle pulse wave velocity as a biomarker of cardiovascular disease risk—A call to action on behalf of VascAgeNet," *Hypertension*, vol. 80, no. 10, pp. 1980–1992, Oct. 2023.

[23] A. Saz-Lara, I. Cavero-Redondo, V. Martínez-Vizcaíno, M. Lucerón-Lucas-Torres, C. Pascual-Morena, and I. Sequí-Domínguez, "Association between arterial stiffness and orthostatic hypotension: A systematic review and meta-analysis," *Frontiers Physiol.*, vol. 14, Apr. 2023, Art. no. 1164519.

[24] A. Valerio et al., "A region-based cross-correlation approach for tonometric carotid–femoral pulse wave velocity assessment," *Biomed. Signal Process. Control*, vol. 93, Jul. 2024, Art. no. 106161. [Online]. Available: https://www.sciencedirect.com/science/article/pii/S1746809424002192

[25] A. Milan et al., "Current assessment of pulse wave velocity," *J. Hypertension*, vol. 37, pp. 1547–1557, Aug. 2019.

[26] H. Gyöngyösi et al., "Comparison of different cardiovascular risk score and pulse wave velocity-based methods for vascular age calculation," *Heart, Lung Circulat.*, vol. 30, no. 11, pp. 1744–1751, Nov. 2021.

[27] K. S. Heffernan, L. Stoner, A. S. London, J. A. Augustine, and W. K. Lefferts, "Estimated pulse wave velocity as a measure of vascular aging," *PLoS ONE*, vol. 18, no. 1, Jan. 2023, Art. no. e0280896.

[28] V. Fabian et al., "Noninvasive assessment of aortic pulse wave velocity by the brachial occlusion-cuff technique: Comparative study," *Sensors*, vol. 19, no. 16, p. 3467, Aug. 2019.

[29] I. Buraioli et al., "A new noninvasive system for clinical pulse wave velocity assessment: The athos device," *IEEE Trans. Biomed. Circuits Syst.*, vol. 15, no. 1, pp. 133–142, Feb. 2021. [Online]. Available: https://www.ieee.org/publications/rights/index.html

[30] D. Leone et al., "Accuracy of a new instrument for noninvasive evaluation of pulse wave velocity: The arterial sTiffness faitHful tOol aSsessment project," *J. Hypertension*, vol. 39, no. 11, pp. 2164–2172, 2021.

[31] D. Said Ouamer, M. K. Guerchani, A. Azaza, and S. Benkhedda, "Arterial stiffness assessed by pulse wave velocity in young athletes practicing endurance or intense resistance training," *Sci. Sports*, vol. 38, no. 3, pp. 266–273, May 2023.

[32] M. Butlin and A. Qasem, "Large artery stiffness assessment using SphygmoCor technology," *Pulse*, vol. 4, no. 4, pp. 180–192, 2016.

[33] A. Sanginario et al., "Live demonstration: Wireless device for pulse wave velocity evaluation," in *Proc. 2023 IEEE Int. Symp. Circuits Syst. (ISCAS)*, May 2023, p. 1.

[34] (1999). *Bluetooth Core Specification Bluetooth ® Specification*. [Online]. Available: https://www.bluetooth.com/specifications/adopted-specifications

[35] *STM32WB15CC Multiprotocol Wireless 32-bit MCU Arm ®-based Cortex ®-M4 With FPU, Bluetooth ® 5.2 Radio Solution Datasheet-Production Data*. Accessed: Apr. 15, 2024. [Online]. Available: https://www.st.com

[36] *Datasheet STLQ020*. Accessed: Apr. 15, 2024. [Online]. Available: https://www.st.com

[37] *Cellevia Batteries LP401235*. [Online]. Available: https://www.tme.eu

[38] *An5165-How To Develop Rf Hardware Using STM32WB Microcontrollers*. Accessed: Apr. 15, 2024. [Online]. Available: https://www.st.com

[39] *Datasheet Nx2012sa Ndk-32.768 Khz Crystal Oscillator*. Accessed: Apr. 15, 2024. [Online]. Available: https://www.ndk.com/en/

[40] *Datasheet Ndk High Speed Crystal Oscillator NX2016SA-32M-EXS00A-CS06465*. Accessed: Apr. 15, 2024. [Online]. Available: https://wwww.honeywell.com

[41] *Datasheet Honeywell Fma Series Fmamsdxx005wcsc3*. Accessed: Apr. 15, 2024. [Online]. Available: https://wwww.honeywell.com

[42] *Datasheet Mcp738312*. Accessed: Apr. 15, 2024. [Online]. Available: https://www.microchip.com

[43] *STM32WB55XX STM32WB35XX Multiprotocol Wireless 32-bit Mcu Arm ®-based Cortex ®-m4 With Fpu, Bluetooth ® 5.3 and 802.15.4 Radio Solution Datasheet-Production Data*. Accessed: Apr. 15, 2024. [Online]. Available: https://www.st.com

[44] Stmicroelectronics. *STM32WB Ble Stack Programming Guidelines—Programming Manual*. Accessed: Apr. 15, 2024. [Online]. Available: https://www.st.com

[45] *How To Build a Bluetooth® Low Energy Mesh Application for Stm32wb Series Microcontrollers*. Accessed: Apr. 15, 2024. [Online]. Available: https://www.st.com

[46] P. Bulić, G. Kojek, and A. Biasizzo, "Data transmission efficiency in Bluetooth low energy versions," *Sensors*, vol. 19, no. 17, p. 3746, Aug. 2019.

[47] D. Demarchi, I. Buraioli, A. Milan, F. Veglio, and F. Vallelonga, "Method and system for real-time measurement of a sphygmic wave velocity," Int. Patent-Priority number: 102 020 000 027 846, Nov. 2020.

[48] *Datasheet NI-USB-6259 Specifications*. Accessed: Apr. 15, 2024. [Online]. Available: https://www.ni.com

[49] M. Ring, M. J. Eriksson, P. Farahnak, L.-O. Farnebo, I.-L. Nilsson, and K. Caidahl, "Arterial stiffness evaluation by SphygmoCor and arteriograph," *Heart, Lung Circulat.*, vol. 17, pp. 16–17, Jan. 2008.

[50] M.-R. Rezai, B. R. Cowan, N. Sherratt, J. D. Finn, F. C. W. Wu, and J. K. Cruickshank, "A magnetic resonance perspective of the pulse wave transit time by the arteriograph device and potential for improving aortic length estimation for central pulse wave velocity," *Blood Pressure Monitor.*, vol. 18, no. 2, pp. 111–118, 2013.

[51] F. Stea, E. Bozec, S. Millasseau, H. Khettab, P. Boutouyrie, and S. Laurent, "Comparison of the complior analyse device with sphygmocor and complior SP for pulse wave velocity and central pressure assessment," *J. Hypertension*, vol. 32, no. 4, pp. 873–880, 2014.

[52] P. Salvi et al., "Noninvasive estimation of aortic stiffness through different approaches," *Hypertension*, vol. 74, no. 1, pp. 117–129, Jul. 2019.

[53] B. Spronck et al., "2024 recommendations for validation of noninvasive arterial pulse wave velocity measurement devices," *Hypertension*, vol. 81, no. 1, pp. 183–192, Jan. 2024.

[54] A. Valerio et al., "Live demonstration: Wireless device for clinical pulse wave velocity evaluations," in *Proc. IEEE Biomed. Circuits Syst. Conf. (BioCAS)*, Oct. 2022, p. 247.

Open Access funding provided by 'Politecnico di Torino' within the CRUI-CARE Agreement